^{68}Ga-DOTANOC PET/CT Allows Somatostatin Receptor Imaging in Idiopathic Pulmonary Fibrosis: Preliminary Results

Valentina Ambrosini[1], Maurizio Zompatori[2], Fiorella De Luca[2], D'Errico Antonia[3], Vincenzo Allegri[1], Cristina Nanni[1], Deborah Malvi[3], Eva Tonveronachi[4], Luca Fasano[4], Mario Fabbri[4], and Stefano Fanti[1]

[1]Nuclear Medicine, Azienda Ospedaliero-Universitaria di Bologna, S. Orsola-Malpighi Hospital, Bologna, Italy; [2]Radiology, Azienda Ospedaliero-Universitaria di Bologna, S. Orsola-Malpighi Hospital, Bologna, Italy; [3]Pathology, Azienda Ospedaliero-Universitaria di Bologna, S. Orsola-Malpighi Hospital, Bologna, Italy; and [4]Respiratory Medicine, Azienda Ospedaliero-Universitaria di Bologna, S. Orsola-Malpighi Hospital, Bologna, Italy.

Interstitial lung diseases include different clinical entities with variable prognoses. Idiopathic pulmonary fibrosis (IPF), the most common, presents the most severe outcome (death within 3–5 y), whereas nonspecific interstitial pneumonia (NSIP) shows a more indolent progression. Preclinical evidence of somatostatin receptor (SSTR) expression on fibroblasts in vitro and in lung fibrosis murine models, coupled with the longer survival of mice with fibrotic lungs treated with agents blocking SSTR, supports the hypothesis of imaging fibroblast activity in vivo by visualization of SSTR with ^{68}Ga-DOTANOC PET/CT. The aim of this study was to evaluate ^{68}Ga-DOTANOC PET/CT in patients with IPF and NSIP. **Methods:** Seven IPF patients and 7 NSIP patients were included in the study. ^{68}Ga-DOTANOC PET/CT and high-resolution CT (HRCT) were performed in all cases by following a standard procedure. PET/CT results were compared with disease sites and extent on HRCT. **Results:** In IPF, ^{68}Ga-DOTANOC uptake was peripheral, subpleural, and directly correlated with pathologic areas on HRCT (subpleural/reticular fibrosis, honeycombing). NSIP patients showed fainter tracer uptake, whereas corresponding HRCT showed areas of ground-glass opacity and rare fibrotic changes. Only IPF patients showed a linear correlation between maximal SUV and disease extent quantified both automatically (Q) (IPF: $P = 0.002$, $R = 0.93$) and using the visual score (Spearman $\rho = 0.46$, $P = 0.0001$). Q directly correlated with percentage carbon monoxide diffusing capacity in IPF ($P = 0.03$, $R = 0.79$) and NSIP ($P = 0.05$, $R = 0.94$), whereas maximal SUV did not present any correlation with percentage carbon monoxide diffusing capacity. **Conclusion:** Our preliminary data show that ^{68}Ga-DOTANOC PET/CT demonstrates SSTR overexpression in IPF patients; this may prove interesting for the evaluation of novel treatments with somatostatin analogs.

Key Words: PET/CT; ^{68}Ga-DOTANOC; IPF; NSIP

J Nucl Med 2010; 51:1950–1955
DOI: 10.2967/jnumed.110.079962

Received Jun. 4, 2010; revision accepted Aug. 30, 2010.
For correspondence or reprints contact: Valentina Ambrosini, Nuclear Medicine, Pad 30, Azienda Ospedaliero Universitaria di Bologna, Policlinico S. Orsola-Malpighi, Via Massarenti 9, 40138, Bologna, Italy.
E-mail: valentina.ambrosini@aosp.bo.it

Interstitial lung diseases (ILDs) are a heterogeneous group of chronic lung disorders including idiopathic entities and secondary forms (*1*). Idiopathic pulmonary fibrosis (IPF) is the most common and is defined by the American Thoracic Society and European Respiratory Society (*1*) as a specific form of chronic fibrosing interstitial pneumonia limited to the lungs and characterized by the histologic hallmark of a usual interstitial pneumonia pattern. Usual interstitial pneumonia histologic features include patchy areas of fibrosis in association with areas with normal lung architecture (*2*); mild inflammatory infiltrate might be present but is not predominant. Fibroblastic foci (aggregates of collagen-producing activated fibroblasts or myofibroblasts) (*3*) are the key histologic feature of IPF, and their presence and extent correlate with a worse disease outcome (*4*).

IPF prognosis is severe, with an invariable progression to end-stage lung disease and death within 3–5 y from diagnosis (*1,5,6*). Most patients show a slowly progressive clinical course (*7*), whereas others experience an acute clinical deterioration in the absence of infectious pneumonia, heart failure, or sepsis (*8*). Proposed treatment options (steroids (*1*), azathioprine (*1*), cyclophosphamide (*1*), interferon γ (*9*), bosentan (*10*), etanercept (*11*), and imatinib (*12*)) are largely ineffective and do not significantly influence the natural history of the disease.

The diagnostic criteria of the American Thoracic Society (*1*) for IPF are based on clinical–radiologic distinctive features and allow a confident diagnosis in typical cases, with pathologic confirmation only in atypical cases. High-resolution CT (HRCT) is the current imaging modality of choice for IPF diagnosis. However, a confident differential diagnosis between IPF and other ILD is influenced by the HRCT reader's experience (*13*). In particular, it is interesting to differentiate IPF from idiopathic interstitial pneumonias showing a more indolent progression, such as nonspecific interstitial pneumonia (NSIP) (*1*).

Although PET is used as the gold-standard imaging modality for the assessment of active disease in oncologic patients, the results obtained using PET in IPF were unsatisfactory with either ^{18}F-FDG (*14*) or ^{18}F-proline (*15*).

Preclinical data (*16*) showed that both murine and human fibroblasts express somatostatin receptors (SSTR) in vitro and in a murine model of bleomycin-induced lung fibrosis. Treatment of fibrotic mice with a somatostatin analog increased mouse survival, improved the pathologic score, and reduced collagen deposition.

Recently, PET tracers specifically binding to SSTR (^{68}Ga-DOTA peptides), have been developed and are used in neuroendocrine tumor clinical trials (*17*) for staging, identifying the unknown primary tumor, and guiding receptor-targeted therapy with either hot or cold somatostatin analogs. Among the different tracers, ^{68}Ga-DOTANOC presents the broader SSTR-subtype affinity (*18*), a favorable dosimetry, and no uptake in the intact lung (*19*).

The aim of our study was to evaluate the potential role of ^{68}Ga-DOTANOC PET/CT in patients with IPF and NSIP. To our knowledge, this is the first report of the use of ^{68}Ga-DOTANOC for noninvasive assessment of SSTR expression in the lungs of IPF patients.

MATERIALS AND METHODS

Patients with IPF or NSIP were prospectively enrolled at the Respiratory Unit of S. Orsola-Malpighi University Hospital, Bologna, Italy, between January 2009 and December 2009. The study was approved by the local Ethical Committee. IPF and NSIP were diagnosed on the basis of the American Thoracic Society radiologic–clinical criteria in all cases (*1*). Overall, 14 cases that had been followed up after the initial diagnosis were included in the study.

Clinical and epidemiologic data were collected in all cases. Smoking habits, environmental and occupational exposure to known fibrogenic drugs, and familial history of fibrotic disorders were recorded.

Lung function tests were obtained in all cases and were performed using a VMAX by Vyasis Healthcare according to the American Thoracic Society/European Respiratory Society Task Force for standardization of lung function testing (*20–23*). The best of 3 reproducible flow–volume loops was chosen; lung volumes were calculated by body plethysmography, and the mean values of 3 repeatable tests were obtained. Carbon monoxide diffusing capacity was calculated with the single-breath technique, using the average of 2 acceptable maneuvers, adjusted for hemoglobin levels. Arterial blood gas samples were taken in seated patients who were breathing room air and had been resting for at least 30 min. Analysis was performed by an ABL Radiometer gas analyzer.

HRCT studies were performed with a 16-detector spiral CT scanner (Somaton Cardiac 16; Siemens Medical Imaging), without injection of contrast material. The patients were studied while supine and while holding their breath at full inspiration, after adequate coaching. The imaging parameters were 90 mA, 120 kVp, a 1.4 pitch, and a 0.5-s rotation time. No respiratory gating was used. CT images were reconstructed at contiguous section widths of 1.25 mm, with a high-spatial-frequency convolutional filter for bone algorithm. CT examinations were anonymized by a radiologist not involved in this study, then independently reviewed by 2 thoracic radiologists, one with extensive experience (30 y) and the other with limited experience (5 y). Neither of the radiologists had knowledge of the clinical data, and they reached the final image interpretation by consensus. The HRCT pattern of IPF consists of patchy, predominantly peripheral, subpleural, bibasal reticular abnormalities with a variable component of ground-glass opacity (usually limited, excluding exacerbation episodes) and subpleural honeycombing. NSIP cases show a pattern of predominant ground-glass opacity with rare areas of reticular changes or microcystic honeycombing. Lung window settings of a width of 1,500 and a level of −500 HU were used. For automatic quantification of the extent of fibrotic disease (Q), the lungs were segmented using a density mask program, −200 HU; Q was evaluated using cutoff values of −400/−700 HU (*24*).

HRCT abnormalities were visually scored at 5 anatomic levels for each lung: aortic arch, tracheal bifurcation, the origin of the apical segmental bronchus of the right lower lobe, the entrance of the lower right pulmonary vein in the left atrium, and a level corresponding to the top of the right hemidiaphragm. The signs of pulmonary fibrosis (ground-glass opacity, honeycombing, reticular abnormalities) and the extent of the interstitial disease were visually estimated on the basis of the preexisting literature. The extent of fibrosis was visually evaluated at each level for each lung using the previously described method on a scale of 0–5 (*25*) for both ground glass and reticular opacity. Ground-glass opacity was scored as follows: 0 = no alveolar disease; 1 = ground-glass opacity involving less than 5% of the lobe (minimal, not normal); 2 = ground-glass opacity involving up to 25% of the lobe; 3 = ground-glass opacity involving from 25% to 49% of the lobe; 4 = ground-glass opacity involving from 50% to 75% of the lobe; and 5 = ground-glass opacity involving more than 75% of the lobe. Interstitial disease was scored as follows: 0 = no interstitial disease; 1 = interlobular septal thickening with no discrete honeycombing; 2 = honeycombing (either with or without associated septal thickening) involving up to 25% of the lobe; 3 = honeycombing (either with or without associated septal thickening) involving from 25% to 49% of the lobe; 4 = honeycombing (either with or without associated septal thickening) involving from 50% to 75% of the lobe; and 5 = honeycombing (either with or without associated septal thickening) involving more than 75% of the lobe. The extent of fibrosis was estimated to the nearest 5% for each lobe, and a mean score was calculated for the whole lung. These scores were also summed into a total CT score. In particular, the final score was obtained by calculating the average score of the 2 observers.

^{68}Ga-DOTANOC PET/CT was performed in all cases within 3 wk of HRCT. ^{68}Ga-DOTANOC was synthesized by the Radiopharmacy of the Nuclear Medicine Unit. ^{68}Ga was eluted from a ^{68}Ge/^{68}Ga generator, and DOTANOC was labeled with ^{68}Ga following the procedure described by Zhernosekov et al. (*26*).

PET/CT was performed 60 min after the intravenous injection of about 180 MBq (120–185 MBq) of ^{68}Ga-DOTANOC using a dedicated PET/CT tomograph (Discovery STE; GE Medical System). PET emission images were recorded for 4 min per bed position in 3-dimensional mode using the Discovery STE. All images in each scan were corrected for scatter, randoms, dead time, and decay. CT acquisition parameters were 120 kV, 60 mA, a 0.8-s tube rotation, and a 5-mm thickness; scaled CT images were used to obtain CT-attenuation-corrected PET images. Low-dose CT was performed without intravenous contrast enhancement. Discovery STE images were reconstructed using a fully 3-dimensional iterative reconstruction algorithm. PET/CT images were read by 2 experienced nuclear medicine specialists, and the final report was based on the readers' consensus. Because both IPF and NSIP are disorders limited to the lungs, the field of view

of all PET/CT scans included only the thorax. In healthy human subjects, there is no ^{68}Ga-DOTANOC uptake in the lungs. Therefore, any area of tracer uptake within the lungs was considered pathologic.

The maximal standardized uptake value (SUVmax) was calculated by measuring the maximal concentration of the labeled tracer in the region of interest and correcting it for patient body weight and injected dose (SUVmax = maximum activity concentration/[injected dose/body weight]). In dealing with a receptor-based tracer, the main interest is to localize areas with higher uptake that reflects higher receptor expression.

^{68}Ga-DOTANOC PET/CT findings were compared with HRCT results in terms of both sites and extent of tracer uptake. SUVmax was also plotted against the extent of disease as measured automatically on HRCT (Q) and was compared with the visual score.

Mean, SD, median, range, and frequencies were used to describe the data. The Spearman rank correlation test was used as indicated between quantitative variables. SPSS software (version 16.0; SPSS Inc.) was used to analyze data. Two-tailed P values of less than 0.05 were considered statistically significant.

RESULTS

Fourteen ILD patients were enrolled (8 men and 6 women; mean age ± SD, 69.6 ± 8.1 y [range, 51–79 y]). In particular, 7 of 14 patients had IPF (all men; mean age, 70.8 ± 5.8 y [range, 63–78 y]) and 7 of 14 had NSIP (1 man and 6 women; mean age, 68.4 ± 10.3 y [range, 51–79 y]). The mean age at diagnosis was 67.7 ± 5.9 y [range, 59–74 y] for IPF patients and 66.7 ± 9.7 y [range, 48–77 y] for NSIP patients.

In 7 patients, pathologic biopsy samples were also available (4/7 IPF and 3/7 NSIP), and the diagnosis was confirmed on the basis of the criteria of the American Thoracic Society.

IPF patients had more severely impaired lung function: pulmonary function test data are reported in detail in Table 1. With the exception of 1 NSIP patient, all patients were receiving therapy at the time of the PET scan (IPF: steroids in 3 cases, steroids and cyclophosphamide in 2 cases, and steroids and azathioprine in 2 cases; NSIP: steroids in 3 cases, steroids and methotrexate in 2 cases, and steroids and azathioprine in 1 case).

In IPF patients, PET/CT showed ^{68}Ga-DOTANOC uptake with a typical subpleural and peripheral distribution (Fig. 1) involving both lung fields predominantly at the lung bases. Areas of ^{68}Ga-DOTANOC uptake directly corresponded to pathologic areas on HRCT. In particular, HRCT scans of IPF showed typical subpleural and peripheral abnormalities, consisting mainly of honeycombing and reticular changes with minimal or absence of ground-glass opacity. The areas of highest ^{68}Ga-DOTANOC uptake corresponded to the border between honeycombing changes and ground-glass opacity.

In contrast, ^{68}Ga-DOTANOC uptake was faint in NSIP patients and undetectable in healthy control subjects (Fig. 2). HRCT scans of NSIP cases showed a pattern of predominant ground-glass opacity with rare areas of reticular changes or microcystic honeycombing.

TABLE 1
Pulmonary Function Test Results

	IPF			NSIP			
	Mean	Median	SD	Mean	Median	SD	P
PaO_2	65.6	59.0	19.9	75.4	71.0	13.9	0.400
FVC	2.3	2.3	1.0	1.7	1.6	0.3	0.030
FVC%	63.9	64.0	21.9	73.7	65.0	17.5	0.460
FEV1	1.8	2.0	0.7	1.4	1.4	0.2	0.007
FEV1%	67.6	75.0	18.1	78.3	70.0	20.7	0.690
FEV1/FVC%	83.5	83.5	9.4	84.9	87.0	6.4	0.440
TLC	3.4	3.7	1.2	2.6	2.5	0.3	0.007
TLC%	52.8	59.0	17.1	63.4	64.0	7.4	0.015
RV	1.0	0.8	0.5	1.1	0.8	0.3	0.630
RV%	44.6	36.0	23.5	46.8	46.0	3.0	0.002
FEF25–75	2.9	2.4	1.5	1.9	1.8	0.5	0.012
FEF25%–75%	98.8	80.0	52.2	67.7	66.0	21.0	0.017
DLCO	9.4	9.2	4.2	7.5	10.9	5.6	0.140
DLCO%	31.3	25.0	13.6	38.4	48.0	29.5	0.010

PaO_2 = arterial oxygen partial pressure; FVC = forced vital capacity; FEV1 = forced expiratory volume in 1 s; TLC = total lung capacity; RV = residual volume; FEF = forced expiratory flow; DLCO = carbon monoxide diffusing capacity.

Only IPF patients showed a linear correlation (Fig. 3) between SUVmax and Q (IPF: $P = 0.002$, $R = 0.93$). Moreover SUVmax was significantly higher at lung levels (Supplemental Table 1) that had more extensive disease (Spearman $\rho = 0.46$, $P = 0.0001$).

Q directly correlated with percentage carbon monoxide diffusing capacity in IPF ($P = 0.03$, $R = 0.79$) and NSIP ($P = 0.05$, $R = 0.94$), but no relationship was observed between SUVmax and percentage carbon monoxide diffusing capacity.

DISCUSSION

PET/CT is successfully used to detect areas of active disease in many forms of human cancer. However, its use in ILD patients has been limited. ^{18}F-FDG PET was used with unsatisfactory results in a few studies investigating small populations of ILD patients. Nusair et al. studied 21 ILD

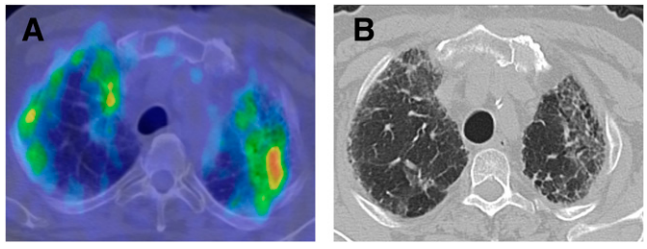

FIGURE 1. ^{68}Ga-DOTANOC PET/CT (A) and HRCT (B) transaxial images of IPF patient. Areas of increased tracer uptake are peripheral and subpleural and correspond to areas of fibrotic abnormalities on HRCT.

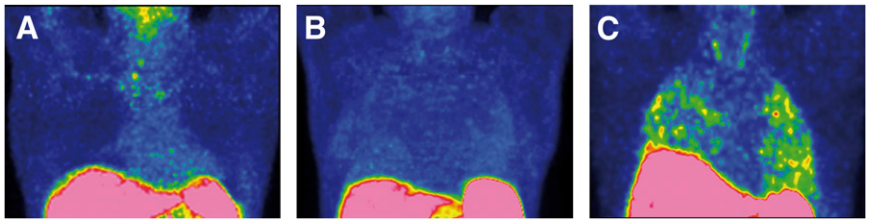

FIGURE 2. ^{68}Ga-DOTANOC PET/CT MIP images of healthy control (A), NSIP patient (B), and IPF patient (C). ^{68}Ga-DOTANOC uptake is evident only in IPF, showing typical peripheral distribution. Only faint uptake is present in NSIP, and no uptake is evident in healthy lungs.

cases (14 IPF, 4 NSIP, 1 respiratory bronchiolitis ILD, 1 sarcoidosis, and 1 Langerhans cells histiocytosis) and reported no differences in mean SUVmax between IPF and non-IPF forms (*14*). Comparable results were obtained by Groves et al. in a population of 36 patients including IPF and heterogeneous non-IPF entities and including both primary forms (4 patients) and secondary forms (asbestos, rheumatoid arthritis, and Sjögren syndrome) (*27*). ^{18}F-proline was also used for ILD PET, but the low lung uptake limited its further use (*15*).

Recent preclinical evidence demonstrated SSTR expression on fibroblasts of both murine models of IPF and human tissue samples from IPF patients (*16*); the authors reported increased SSTR 2 receptor messenger RNA expression after bleomycin intratracheal murine instillation.

Evidence of a human in vivo correlate to these preclinical findings may be derived from a few isolated reports in the literature that confirm that fibrotic lungs present SSTR expression. SSR scintigraphy was falsely positive in a patient with pulmonary fibrosis (*28*), and positive SSR scintigraphy findings in IPF cases have been reported to correlate with disease progression (*29*).

To our knowledge, PET tracers targeting SSTR have never been used in ILD patients.

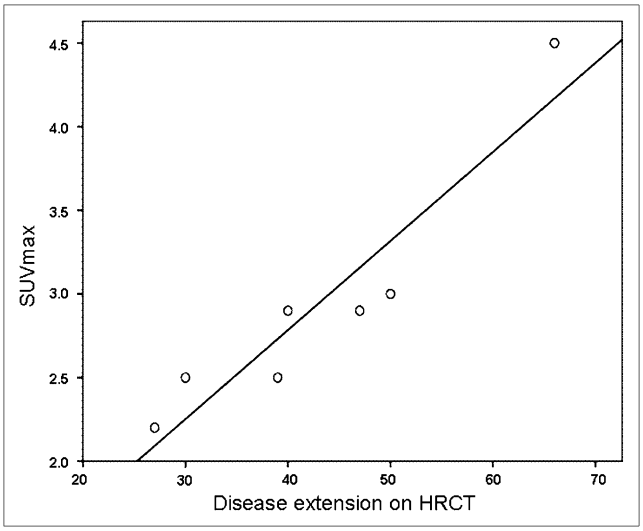

FIGURE 3. Linear correlation ($P = 0.002$, $R = 0.93$) between ^{68}Ga-DOTANOC PET/CT SUVmax and disease extent automatically assessed on HRCT.

^{68}Ga-DOTANOC presents a high affinity for SSTR 2, 3, and 5 and is currently used in several centers for neuroendocrine tumor imaging (*17*) with good results.

Our preliminary data showed that IPF patients presented characteristic peripheral and subpleural ^{68}Ga-DOTANOC uptake that directly corresponded to areas of HRCT abnormalities. No significant tracer uptake was observed in NSIP patients, whereas normal lungs did not show any ^{68}Ga-DOTANOC uptake.

A strong linear correlation was found between the SUVmax of IPF cases and disease extent on HRCT, quantified by both the automatic and the visual score. In contrast, no significant association was documented in NSIP cases.

Overall, our preliminary data support SSTR overexpression within IPF lungs, in accordance with preclinical data.

It can be debated that this study was limited by the lack of immunohistochemistry confirmation of the precise cellular localization of SSTR within the lungs of IPF patients. However, obtaining a pathologic sample from patients with IPF is extremely difficult because current guidelines do not recommend biopsy in typically presenting cases (*1,30*). Various human normal lung cells have been reported to express SSTR 2A (alveolar type 2 pneumocytes, epithelial cells, smooth muscle cells, alveolar macrophages, and some endothelial cells) (*16*). Moreover, SSTR expression coupled with G-protein signal transduction was demonstrated in human fetal lung fibroblasts, and G-proteins were reported to be involved in cellular proliferation and differentiation mechanisms in lung injury and repair (*31*).

Although ^{68}Ga-DOTANOC binding sites within the lungs cannot be precisely localized without direct sampling, the evidence that tracer uptake was observed only in IPF cases allows one to speculate that PET with ^{68}Ga-DOTANOC might be useful to identify SSTR overexpression in this patient subgroup. This observation may support a new field of research focused on the role of SSTR in IPF pathogenesis and treatment.

Current understanding of IPF pathogenesis is poor, and the precise factors that initiate and maintain pulmonary fibrosis are unknown. The clinical insidious onset and relentless progression of IPF coupled with the temporally heterogeneous appearance of the usual interstitial pneumonia pattern supports the hypothesis that IPF may follow subsequent episodes of epithelial injury, followed by abnormal tissue repair (*32*). In this view, fibroblastic foci have been suggested to represent an organizing phase of focal acute lung injury. Recent studies indicate that myofibroblasts may orig-

inate from resident fibroblasts (*33*), circulating fibrocytes (*34*), bone marrow–derived fibroblast precursors (*35*), and lung epithelial cells via epithelial–mesenchymal transition (*36*). In fact, fibroblastic foci are located mainly in a transition zone between abnormal fibrotic lung and uninvolved areas and are currently considered the leading edge of fibrosis, extending from the subpleural regions to the lung parenchyma. Another recent hypothesis describes the disease as a cancerlike syndrome of dysregulated fibroblasts (*37*).

Interestingly, in our limited IPF population, ^{68}Ga-DOTANOC uptake was more intense at the border between honeycombing changes and areas of ground-glass opacity, where fibroblastic foci are most represented.

^{68}Ga-DOTANOC PET/CT is currently used to select neuroendocrine tumor patients for treatment with cold or hot somatostatin analogs (diagnostic compounds labeled with isotopes that selectively destroy SSTR-expressing cells). ^{68}Ga-DOTANOC PET/CT might be used for this indication also in IPF patients, selecting those who might benefit from somatostatin analog treatment or combined approaches in which ^{68}Ga-DOTANOC may function as a carrier for specific antifibrotic drugs or cytotoxic isotopes. Activation of SSTR by somatostatin analogs was recently reported to be associated with improved survival of fibrotic mice (69%), compared with untreated controls (44%); improved pathologic scores; and reduced collagen deposition and lung inflammation (*16*). In vitro studies showed that somatostatin promoted fibroblast apoptosis through its SSTR 2 receptor (*38*) whereas octreotide showed inhibitory effects on fibrosis development and fibroblast proliferation in several preclinical models (*39,40*).

CONCLUSION

Our preliminary data showed that ^{68}Ga-DOTANOC uptake corresponded to areas of HRCT abnormalities in IPF patients, supporting the hypothesis that SSTR is overexpressed in the lungs of IPF patients. Considering the poor prognosis of IPF and that known treatments are largely ineffective, these observations may lead to the delineation of new treatment approaches using somatostatin analogs. It would also be interesting to evaluate if PET data on SSTR expression correlate with the observed differences in disease prognosis in other forms of ILD (both idiopathic and secondary).

REFERENCES

1. American Thoracic Society. Idiopathic pulmonary fibrosis: diagnosis and treatment. International consensus statement. American Thoracic Society (ATS) and the European Respiratory Society (ERS). *Am J Respir Crit Care Med.* 2000; 161:646–664.
2. Flaherty KR, Travis WD, Colby TV, et al. Histopathologic variability in usual and non-specific interstitial pneumonias. *Am J Respir Crit Care Med.* 2001;164: 1722–1727.
3. Katzenstein AL, Myers JL. Idiopathic pulmonary fibrosis: clinical relevance of pathologic classification. *Am J Respir Crit Care Med.* 1998;157:1301–1315.
4. King TE Jr, Schwarz MI, Brown K, et al. Idiopathic pulmonary fibrosis: relationship between histopathologic features and mortality. *Am J Respir Crit Care Med.* 2001;164:1025–1032.
5. Coultas DB, Zumwalt RE, Black WC, Sobonya RE. The epidemiology of interstitial lung disease. *Am J Respir Crit Care Med.* 1994;150:967–972.
6. Panos RJ, Mortenson R, Niccoli SA, King TE Jr. Clinical deterioration in patients with idiopathic pulmonary fibrosis: causes and assessment. *Am J Med.* 1990;88:396–404.
7. Martinez FJ, Safrin S, Weycker D, et al., for the IPF Study Group. The clinical course of patients with idiopathic pulmonary fibrosis. *Ann Intern Med.* 2005; 142:963–996.
8. Collard HR, Moore BB, Flaherty KR, et al., for the Idiopathic Pulmonary Fibrosis Clinical Research Network Investigators. Acute exacerbations of idiopathic pulmonary fibrosis. *Am J Respir Crit Care Med.* 2007;176:636–643.
9. Raghu G, Brown KK, Bradford WZ, et al. A placebo-controlled trial of interferon gamma-1b in patients with idiopathic pulmonary fibrosis. *N Engl J Med.* 2004;350:125–133.
10. King TE Jr, Behr J, Brown KK, et al. BUILD-1: a randomized placebo-controlled trial of bosentan in idiopathic pulmonary fibrosis. *Am J Respir Crit Care Med.* 2008;177:75–81.
11. Raghu G, Brown KK, Costabel U, et al. Treatment of idiopathic pulmonary fibrosis with etanercept: an exploratory, placebo-controlled trial. *Am J Respir Crit Care Med.* 2008;178:948–955.
12. Daniels CE, Lasky JA, Limper AH, et al., for the Imatinib-IPF Study Investigators. Imatinib treatment for idiopathic pulmonary fibrosis: randomized placebo-controlled trial results. *Am J Respir Crit Care Med.* 2010;181:604–610.
13. Grenier P, Valeyre D, Cluzel P, Brauner MW, Lenoir S, Chastang C. Chronic diffuse interstitial lung disease: diagnostic value of chest radiography and high-resolution CT. *Radiology.* 1991;179:123–132.
14. Nusair S, Rubinstein R, Freedman NM, et al. Positron emission tomography in interstitial lung disease. *Respirology.* 2007;12:843–847.
15. Lavalaye J, Grutters JC, van de Garde EM, et al. Imaging of fibrogenesis in patients with idiopathic pulmonary fibrosis with cis-4-[^{18}F]-fluoro-L: -proline PET. *Mol Imaging Biol.* 2009;11:123–127.
16. Borie R, Fabre A, Prost F, et al. Activation of somatostatin receptors attenuates pulmonary fibrosis. *Thorax.* 2008;63:251–258.
17. Ambrosini V, Campana D, Bodei L, et al. ^{68}Ga-DOTANOC PET/CT clinical impact in patients with neuroendocrine tumors. *J Nucl Med.* 2010;51:669–673.
18. Antunes P, Ginj M, Zhang H, et al. Are radiogallium-labelled DOTA-conjugated somatostatin analogues superior to those labelled with other radiometals? *Eur J Nucl Med Mol Imaging.* 2007;34:982–993.
19. Pettinato C, Sarnelli A, Di Donna M, et al. ^{68}Ga-DOTANOC: biodistribution and dosimetry in patients affected by neuroendocrine tumors. *Eur J Nucl Med Mol Imaging.* 2008;35:72–79.
20. Miller MR, Crapo R, Hankinson J, et al., for the ATS/ERS Task Force. General considerations for lung function testing. *Eur Respir J.* 2005;26:153–161.
21. Miller MR, Hankinson J, Brusasco V, et al., for the ATS/ERS Task Force. Standardisation of spirometry. *Eur Respir J.* 2005;26:319–338.
22. Wanger J, Clausen JL, Coates A, et al. Standardisation of the measurement of lung volumes. *Eur Respir J.* 2005;26:511–522.
23. Macintyre N, Crapo RO, Viegi G, et al. Standardisation of the single-breath determination of carbon monoxide uptake in the lung. *Eur Respir J.* 2005; 26:720–735.
24. Sverzellati N, Zompatori M, De Luca G, et al. Evaluation of quantitative CT indexes in idiopathic interstitial pneumonitis using a low-dose technique. *Eur J Radiol.* 2005;56:370–375.
25. Gay SE, Kazerooni EA, Toews GB, et al. Idiopathic pulmonary fibrosis: predicting response to therapy and survival. *Am J Respir Crit Care Med.* 1998;157: 1063–1072.
26. Zhernosekov KP, Filosofov DV, Baum RP, et al. Processing of generator-produced ^{68}Ga for medical application. *J Nucl Med.* 2007;48:1741–1748.
27. Groves AM, Win T, Screaton NJ, et al. Idiopathic pulmonary fibrosis and diffuse parenchymal lung disease: implications from initial experience with ^{18}F-FDG PET/CT. *J Nucl Med.* 2009;50:538–545.
28. Ha L, Mansberg R, Nguyen D, Bui C. Increased activity on In-111 octreotide imaging due to radiation fibrosis. *Clin Nucl Med.* 2008;33:46–48.
29. Lebtahi R, Moreau S, Marchand-Adam S, et al. Increased uptake of ^{111}In-octreotide in idiopathic pulmonary fibrosis. *J Nucl Med.* 2006;47:1281–1287.
30. Hunninghake GW, Zimmerman MB, Schwartz DA, et al. Utility of lung biopsy in the diagnosis of idiopathic pulmonary fibrosis. *Am J Respir Crit Care Med.* 2001;164:193–196.
31. Busto R, Carrero I, Zapata P, Colás B, Prieto JC. Identification of functional somatostatin receptors and G-proteins in a new line of human foetal lung fibroblasts. *Endocr Res.* 2000;26:477–486.
32. Selman M, King TE, Pardo A. Idiopathic pulmonary fibrosis: prevailing and evolving hypotheses about its pathogenesis and implications for therapy. *Ann Intern Med.* 2001;134:136–151.

33. Phan SH. The myofibroblast in pulmonary fibrosis. *Chest.* 2002;122(suppl): 286S–289S.
34. Moore BB, Kolodsick JE, Thannickal VJ, et al. CCR2-mediated recruitment of fibrocytes to the alveolar space after fibrotic injury. *Am J Pathol.* 2005;166:675–684.
35. Hashimoto N, Jin H, Liu T, Chensue SW, Phan SH. Bone marrow-derived progenitor cells in pulmonary fibrosis. *J Clin Invest.* 2004;113:243–252.
36. Kasai H, Allen JT, Mason RM, Kamimura T, Zhang Z. TGF-beta1 induces human alveolar epithelial to mesenchymal cell transition (EMT). *Respir Res.* 2005;6:56.
37. Vancheri C, Failla M, Crimi N, Raghu G. Idiopathic pulmonary fibrosis: a disease with similarities and links to cancer biology. *Eur Respir J.* 2010;35:496–504.
38. Guillermet-Guibert J, Saint-Laurent N, Davenne L, et al. Novel synergistic mechanism for sst2 somatostatin and TNFalpha receptors to induce apoptosis: crosstalk between NF-kappaB and JNK pathways. *Cell Death Differ.* 2007; 14:197–208.
39. Wang J, Zheng H, Hauer-Jensen M. Influence of short-term octreotide administration on chronic tissue injury, transforming growth factor beta (TGF-beta) overexpression, and collagen accumulation in irradiated rat intestine. *J Pharmacol Exp Ther.* 2001;297:35–42.
40. Lahlou H, Saint-Laurent N, Estève JP, et al. SST2 somatostatin receptor inhibits cell proliferation through Ras-, rap1-, and B-Raf-dependent ERK2 activation. *J Biol Chem.* 2003;278:39356–39371.

JNM The Journal of NUCLEAR MEDICINE

^{68}Ga-DOTANOC PET/CT Allows Somatostatin Receptor Imaging in Idiopathic Pulmonary Fibrosis: Preliminary Results

Valentina Ambrosini, Maurizio Zompatori, Fiorella De Luca, D'Errico Antonia, Vincenzo Allegri, Cristina Nanni, Deborah Malvi, Eva Tonveronachi, Luca Fasano, Mario Fabbri and Stefano Fanti

J Nucl Med. 2010;51:1950-1955.
Published online: November 15, 2010.
Doi: 10.2967/jnumed.110.079962

The Journal of Nuclear Medicine is published monthly.
SNMMI | Society of Nuclear Medicine and Molecular Imaging
1850 Samuel Morse Drive, Reston, VA 20190.
(Print ISSN: 0161-5505, Online ISSN: 2159-662X)

SNMMI SOCIETY OF NUCLEAR MEDICINE AND MOLECULAR IMAGING